IJCRT.ORG ISSN : 2320-2882

INTERNATIONAL JOURNAL OF CREATIVE RESEARCH THOUGHTS (IJCRT)

An International Open Access, Peer-reviewed, Refereed Journal

Effect of Self-trapping and Space Charge Polarization in Green Synthesized Cerium Oxide Nanoparticle

[1]Jaya M Soney, [2]Dhannia T,

[1]Research Scholar, [2]Associate Professor,
[1]Physics Department,
[1]Cochin University of Science and Technology, Cochin, India

Abstract: This paper reports the green synthesis of CeO_2 nanoparticles by microwave irradiation method, with freshly prepared egg white. This method is simple, cost-effective, and environment friendly, using $CeCl_3.7H_2O$ and ovalbumin in an aqueous medium. As prepared samples are characterized by XRD, TEM, SEM, FTIR, Raman and DRS. XRD and Raman studies confirm the formation of nanoparticles. TEM result shows rectangular rod shaped polycrystalline nanoparticle formation. Thermal stability is studied using TGA results. PL studies show the various emission peaks and an intensity variation with temperature. PL results give information about the self-trapping exciton mechanism. It also gives information about the hopping of electrons from different defects level to 2p state of oxygen. From DRS results, the band gap of cerium oxide nanoparticles is found to be 3.21eV. Dielectric constant, dielectric loss & AC conductivity of the cerium oxide nanoparticles increases up to 310K and then begin to decreases due to space charge polarization effect at the grain boundary.

Index Terms **- Green synthesis · Ovalbumin · Polaron · Hopping mechanism · self-trapping excitation.**

I. INTRODUCTION

Research in Nanoscience and Nanotechnology has very much importance because of its various applications like health care, nanomedicine, food technology etc. Materials or structures possess new physical properties on the nanometer scale. The applications of nanomaterials utilize size, shape, chemical composition and surface dependent properties. Particles with a size, smaller than the wavelength of visible light have essential applications in material science. Advanced tools and techniques enable us to make new devices in size domain 0.1nm to 50nm.

Due to wide applications such as three-way catalysts, solid oxide fuel cells, filters, gas sensors etc., cerium plays a vital role in material science (Yang et al. 2007) Ceria is the second element in the Lanthanide series having high reactivity, low ionization potential, and less toxic. Cerium oxide is an n-type semiconductor material with bandgap 3.18eV. Cerium oxide nanoparticles are synthesized by many techniques such as chemical preparation, microwave techniques, thermal hydrolysis, co-precipitation process, combustion method etc. Precipitation method is more attractive due to simple operation and cheap salt precursors (Chen et al. 2004).

In this paper, we attempted to study ceria nanoparticles, synthesized using cerium chloride, ammonia and ovalbumin (egg white). Egg white acts as a green binding agent for the preparation of cerium oxide nanoparticles. Here electrostatic interaction between cerium cation and oppositely charged protein takes place, which leads to the controllable growth and isotropic formation of small and stable cerium oxide nanoparticle (Singh et al. 2005, Kargar et al. 2015) Microwave generate high power densities, decreased production cost with efficient production, more compact, controllable, and less ON and OFF time. It is a non-contact drying technology. It is a new approach for synthesizing nanocrystalline ceria, since this technique has not been persude previously.

2. EXPERIMENT

The aqueous solution of 0.1M of cerium oxide (Ce_2O) is prepared by mixing appropriate amount of aqueous cerium chloride ($CeCl_3.7H_2O$) in 250ml of distilled water and 5ml of freshly prepared egg white in 25ml of distilled water. The resultant solution is stirred using magnetic stirrer keeping 500rpm under room temperature for 1 hour. Liquid ammonia is added drop wise to maintain the pH value as 10. The precipitate is washed many times in double distilled water till no chlorine ions are detected. Then washed with ethanol to remove NH^{+3}. The obtained precipitate is irradiated with Microwave for 10 minutes with radiation frequency 1250 GHz and the power up to 1200 Watt. The sample is annealed at different temperatures up to 750^0C (LOGESWARAN et al. 2013).
The particle size and morphology of the samples are characterized by XRD using X Pert PRO PANalytical with $\lambda = 0.154060$nm. The particle size and morphology of the samples are characterized by Transmission Electron Microscope [Joel JEM 2100]. Band gap energies are measured using JASCO V 570 UV-VIS NIR spectrophotometer. Photoluminescence spectra are studied using JASCO FP 8500 spectrofluorometer. FT-IR studies are done using FT-IR Spectrometer (Thermo Nicolet Avatar 370).Raman study is done using Horiba Jobin Yvon Lab RAM HR system equipped with He Ne laser (514 nm wavelength). Dielectric studies are done using

HEWLETT PACKARD 4285A 75 kHz- 300 MHz PRECISION LCR METER. Thermal analysis is done using Perkin Elmer STA 6000.

3. RESULTS and DISCUSSIONS

3.1 XRD analysis

X -Ray Diffraction of the as-prepared and annealed cerium oxide samples are shown in figure 1. The observed broad peaks in the as-prepared samples indicate the formation of nanocrystalline structure of cerium oxide. High intensity diffraction peaks are observed at 28.386, 32.90, 47.346, 56.211, 69.713, 76.566 degrees respective to the planes (111), (200), (220), (311), (400), and (331). The peaks become gradually sharpened with increase in annealing temperature. This indicates, the improvement in the crystallinity of the as-prepared sample by the annealing process (Dhannia et al. 2009, Dhannia et al. 2010).

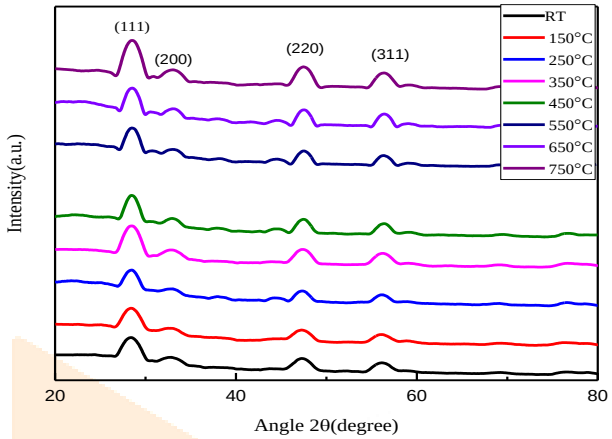

Fig. 1 XRD pattern of the as-prepared and annealed samples

The lattice parameter of the as-prepared cerium oxide nanoparticles is calculated using Bragg's formula (Cullity 1978),

$$2d\sin\theta = n\lambda \qquad (1)$$

λ is the wavelength of X-ray, d is the distance between two planes. In the present investigation the lattice parameter of the as-prepared nanoparticle is calculated as 5.425 A^0. Calculated values are well agreed with that of the JCPDS standard values (81-0792). From XRD data, calculated lattice parameter is found to decrease with increase in temperature. This shows the presence of defects and impurities. Such defects are introduced during the sample preparation and vary according to methods and reagents used (Morris et al 2006)

The average size of the nanocrystal is calculated using the Scherrer formula (Cullity 1978),

$$D = \frac{0.9\lambda}{\beta \cos\theta} \qquad (2)$$

Where 'λ' is the wavelength of X-Ray (0.154060nm), 'β' is FWHM (full width at half maximum), 'θ' is the diffraction angle, and 'D' is grain size.

Sample	Lattice parameter(A^0)	Grain size(nm)
As-prepared	5.425	5.10
Annealed at 150^{0}C	5.422	5.35
Annealed at 250^{0}C	5.417	5.64
Annealed at 350^{0}C	5.415	6.47
Annealed at 450^{0}C	5.409	7.90
Annealed at 550^{0}C	5.403	8.23
Annealed at 650^{0}C	5.398	9.88
Annealed at 750^{0}C	5.384	13.17

Table 1 Variation of lattice parameter and grain size with temperature

From the table 1 the average size of the as-prepared nanoparticle is found to be 5.10nm. It is increased with increase in annealing temperature.

3.2 TEM analysis

The TEM image of the as-prepared sample is shown in figure 2. The SAED ring pattern confirms the polycrystalline fluorite structure of the cerium oxide nanocrystal (Li et al. 2005). The rod-like structure of the particles is found in the as-prepared sample. The TEM results also confirm that the grains are nanometer in size.

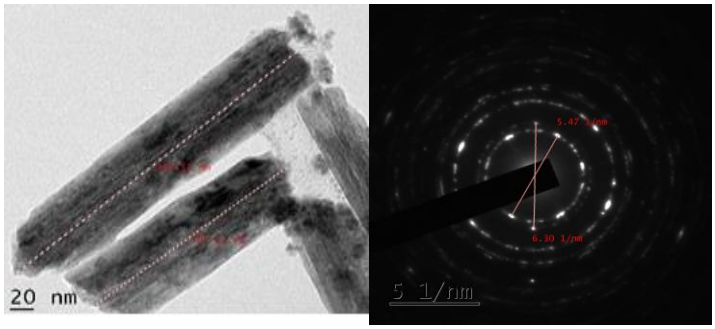

Fig. 2 TEM images of as-prepared sample

3.3 SEM analysis

SEM analysis gives information about the morphology and size of the microcrystalline fluorite structure of CeO_2 nanoparticles. Rectangular rod shaped particles are observed in the SEM image of the as prepared sample. The formation of rod-like and spherical crystallites depends on the pH value of the solution in the course of Ce^{3+}/Ce^{4+} conversion and the reaction mechanism in acid, and alkaline solution obeys the precipitation and decomposition mechanism (Yan et al. 2007). Agglomeration of nanoparticles is a common phenomenon that occurs because, the nanoparticles tend to decrease the exposed surface to lower the surface energy and smaller particle size results in stronger agglomeration (Hu et al. 2006). Wires with large aspect ratios greater than 20 (length to diameter ratio) are called nanowires and those with small aspect ratios are called nanorods. The SEM images of the as-prepared samples is in Figure 3 reveals the formation of nanorods of various sizes with aspect ratio less than 20 (Theivasanthi et al. 2012). The average length of rod is 300nm and diameter is 80nm with aspect ratio 3.75.

The EDX of the as-prepared cerium oxide nanocrystal is shown in figure 4. It confirms the presence of cerium and oxygen. There are no other impurity peaks in this spectrum.

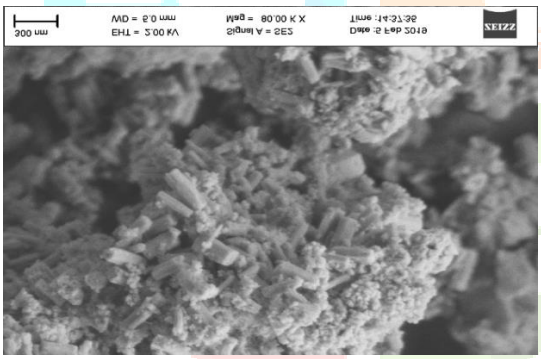

Fig. 3 SEM image of the as prepared sample

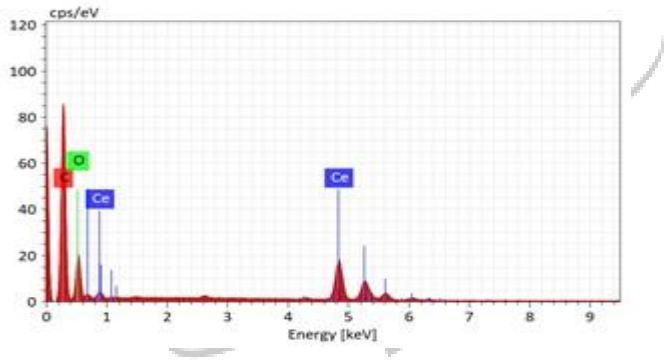

Fig. 4 EDX of the as prepared sample

3.4 FT-IR analysis

The FT-IR spectrum in the transmission mode of the as-prepared sample is shown in figure 5. The broad transmission band in the region around 3400cm^{-1} is due to the presence of surface water. In the region below 1800cm^{-1}, some peaks are found due to the carbonation of ceria (Sujana et al. 2008). Below 500 cm^{-1} prominent stretching Ce-O has been observed due to the formation of cerium oxide (Dos Santos et al. 2008).

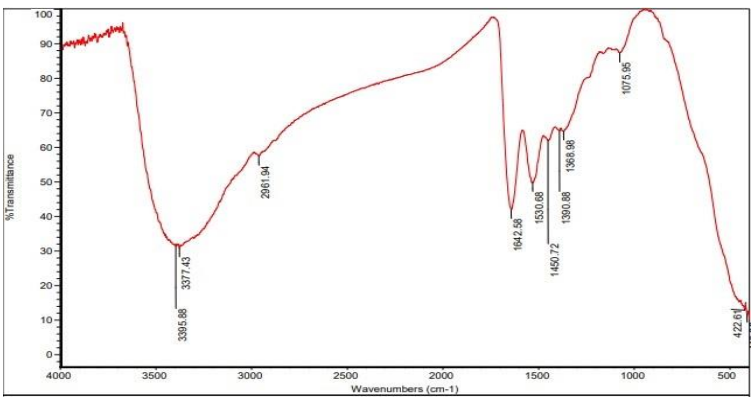

Fig. 5 FTIR spectrum of the as prepared samples

3.5 TGA/DTA analysis

TGA/DTA is carried out between the temperatures 400^{0}C to 800^{0}C. Figure 6 gives the TGA/DTA results of the as-prepared sample. The as-prepared sample shows small weight loss up to 100^{0}C due to the surface absorbed water molecules. The mass loss around 200^{0}C to 300^{0}C is due to the decomposition of bioactive organic molecules from ovalbumin (Maensiri et al. 2007). These organic molecules attached to the surface acts as a capping agent. At higher temperature region around 600^{0}C, a small change in mass is observed due to O_2 loss. When the temperature exceeds 600^{0}C, the as-prepared cerium oxide nanoparticles are transformed to more crystalline form. These results are more clear from the derivative weight % graph.

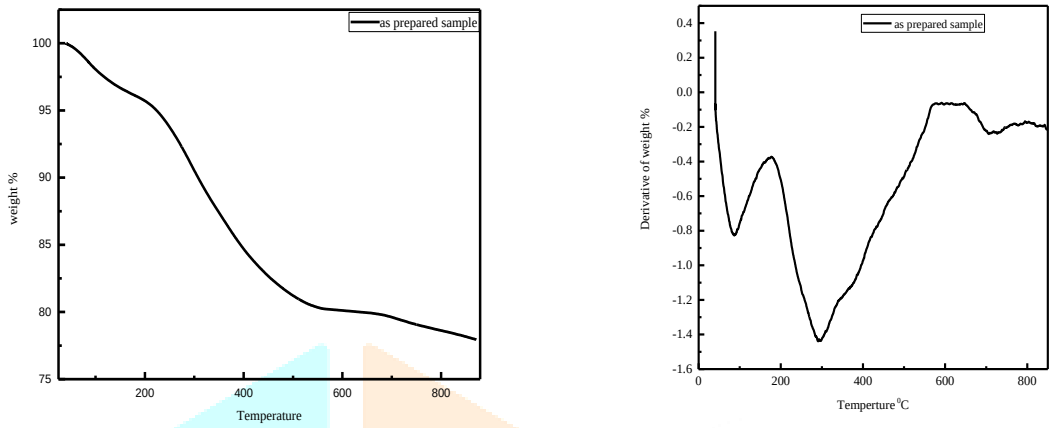

(a) Weight % with temperature of as-prepared sample (b) Derivative of weight % with temperature

Figure 6: Weight % and Derivative of weight % of the as-prepared sample with temperature

3.5 Raman studies

The Raman spectrum of the as-prepared sample is shown in figure 7. The Raman active mode obtained for the as-prepared sample is at 461cm^{-1}. This results from the symmetrical stretching mode of the Ce-O vibrational units, and is sensitive to any disorder in oxygen sublattice and grain size induced nonstoichmetry (Maensiri et al. 2007, Krishnan et al. 2013).

$$\Gamma\ (\mathrm{cm}^{-1}) = 10 + \frac{124.7}{D} \qquad (3)$$

Where Γ (cm^{-1}) is the full width half maximum of the Raman active mode peak and D is the particle size. Calculated particle size from Raman spectra are 3.25, 4.23, 4.86, 6.05, 7.74, 8.94, 10.15, and 13.4nm respectively. The size of the nanoparticles agree well with the XRD results.

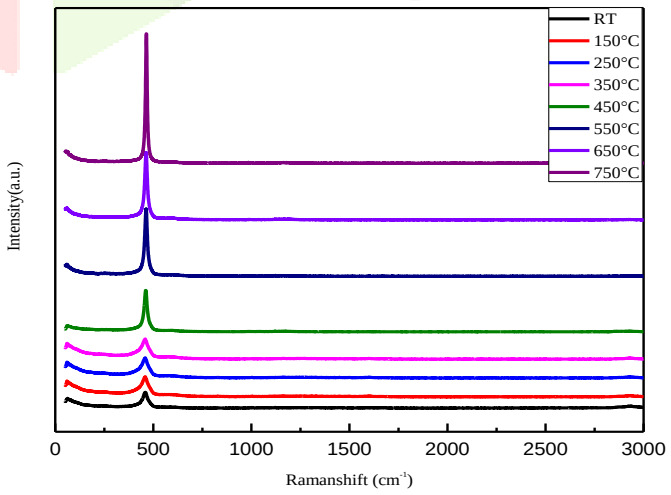

Fig. 7 Raman spectra of the as-prepared and annealed sample

3.6 UV-Vis studies

UV-Vis diffuse reflectance spectra of the as-prepared and annealed cerium oxide samples are shown in figure (8a). It shows strong absorption peaks below 500nm. Absorption peaks decrease with wavelength and the steepness of the curve increases with increase in temperature. When the temperature increases, the absorption edge slightly shifts towards the longer wavelength side, resulting in a slight decrease in the band gap energy (Chen et al. 2005, Zhang et al. 2006). When temperature increases wavelength begins to decrease. At lower temperature, concentration of Ce^{3+} ions increases and thereby increasing the oxygen vacancy. This results in a decrease of absorption wavelength. At higher temperature, the concentration of Ce^{3+} ions decreases and thus it decreases the oxygen vacancy and this results in higher wavelength absorption (Phoka et al. 2009). The absorption peak in figure (8b) is maximum around the wavelength of 320 nm, which shows the intrinsic nature of cerium oxide. When charge transferred from 2p orbital of oxygen to 4f orbital of cerium, fundamental absorption takes place, which gives the band gap value 3.18 eV for the bulk (Truffault et al. 2010). The absorption coefficients of the sample are calculated using Munk-Kublekare relation,

$$\frac{k}{s} = \frac{(1-R)^2}{2R}$$

R is the diffuse reflectivity from an infinitely thick layer of the powder, k is the absorption coefficient, and s is the scattering factor independent of the wavelength for the particle sizes larger than the wavelength.

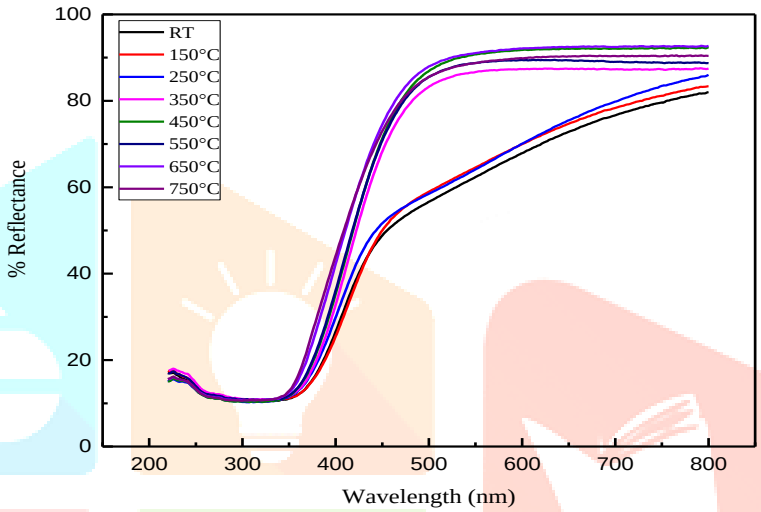

(a) % Reflectance with wavelength

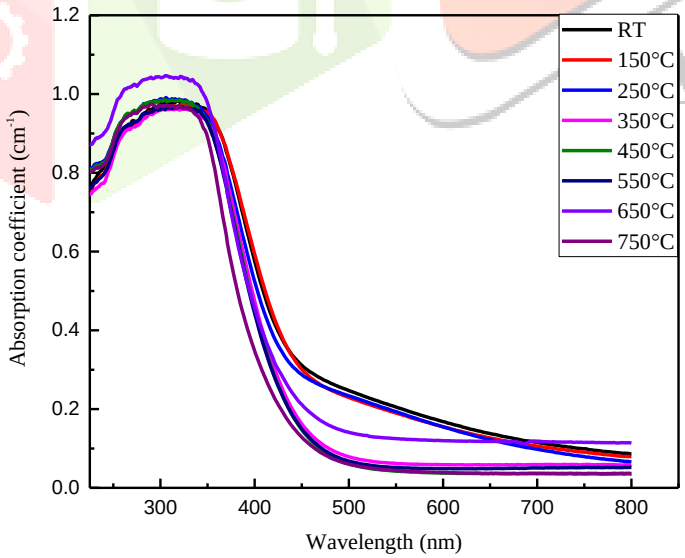

(b) Absorbance with wavelength

Figure 8: (a) %Reflectance and (b) Absorbance of the as-prepared and annealed samples with wavelength.

Direct bandgap energy can be calculated using the equation,

$$\frac{k}{s} h\nu = A\,(h\nu - Eg)^n \qquad (5)$$

By extrapolating the curve $(kh\nu)/s)^2$ vs. (hν) to zero absorption (Tauc plot) as shown in the figure (9a), the value of direct band gap energy obtained for the as-prepared sample is Eg= 3.240 eV. By plotting $(kh\nu/s)^{1/2}$ as a function of photon energy (hν), and extrapolating the linear portion of the curve to zero as in figure (9b), the indirect band gap energy of the as-prepared sample is calculated as Eg = 3.225 eV (Sathyamurthy et al. 2005)

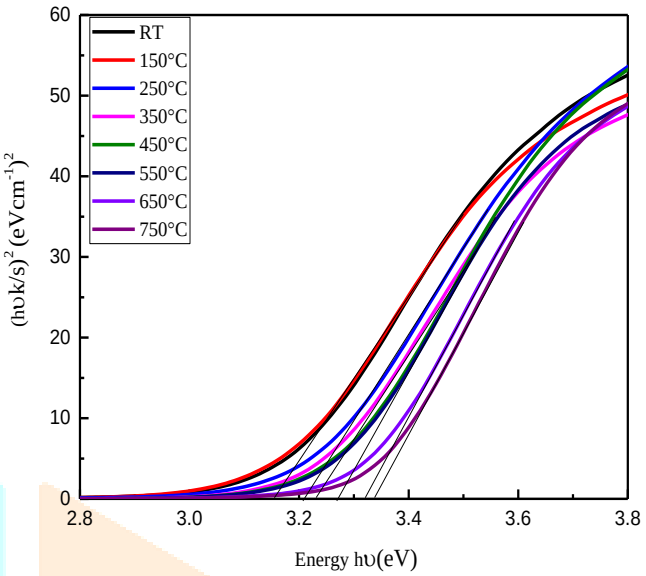

(a)Direct bandgap Energy

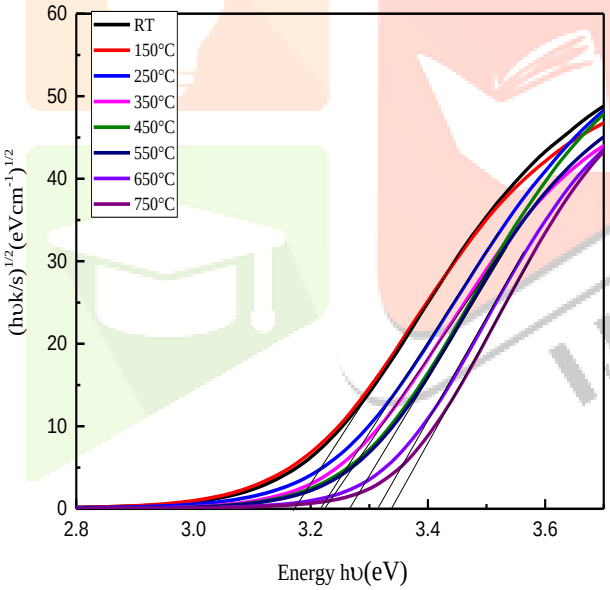

(b) Indirect bandgap energy

Figure 9: (a) Direct and (b) Indirect bandgap Energy of the as-prepared and annealed samples with Energy (h*ν*)

Sample	Direct Bandgap(eV)	Indirect Bandgap (eV)
as-prepared	3.150	3.168
annealed at 150^0 C	3.153	3.170
annealed at 250^0C	3.207	3.213
annealed at 350^0C	3.227	3.224
annealed at 450^0C	3.267	3.263
annealed at 550^0C	3.269	3.264
annealed at 650^0C	3.316	3.321
annealed at 750^0C	3.334	3.333

Table 2 Direct and Indirect bandgap energies of the as-prepared and annealed samples

Ultraviolet radiation from the sun consists of radiations of type A and type B. Type A UV radiations are ranging from 320-400 nm and type B UV radiations are ranging from 290-320nm. UV radiations are the major cause of skin cancers, so filtration of UV radiation is very necessary. Type B UV radiations can be filtered using TiO_2. So nanostructured TiO_2 is widely used in sun screen cosmetic products (Truffault et al 2010). In the present green synthesis method the band gap of nanostructured ceria is found to be of the order of 3.240 eV. So the as prepared nanostructured ceria can be used for the filtration of type A and type B radiations. Good transparency in the visible region and its non-toxicity are the two important characteristics of the as-prepared nanostructured ceria for the application of new generation inorganic ultraviolet filters.

3.7 Optical Studies

Lattice distortion and oxygen deficiency of the as prepared samples are studied using photoluminescence spectrum. This investigation gives the emission property of the as-prepared sample. PL studies of cerium oxide sample at room temperature using excitation wavelength at 320nm is shown in figure 10. The emission peaks are located at 360nm (3.44eV), 398nm (3.11eV), 453nm (2.73eV), 468nm (2.64eV), 483nm (2.56eV), 493nm (2.51eV) and 648nm (1.91eV). The emission peaks from 400nm to 700nm gives hopping from different defects level to 2p state of oxygen. Peaks at 360nm (3.44eV) is due to the hopping of electron from the 4f state of cerium to 2p state of oxygen. A broad UV emission band at 398nm (3.11eV), weak blue bands at 453nm (2.73eV) & 468nm (2.64eV), blue band at 483nm (2.56eV), a weak blue-green band at 493nm (2.51eV) and a weak red band at 648nm (1.91eV) are also observed. This observed peaks are due to the surface defects of the cerium oxide samples. The low-density oxygen vacancies while preparing the cerium oxide sample results in weak intensity green emission (Patsalas et al. 2003).

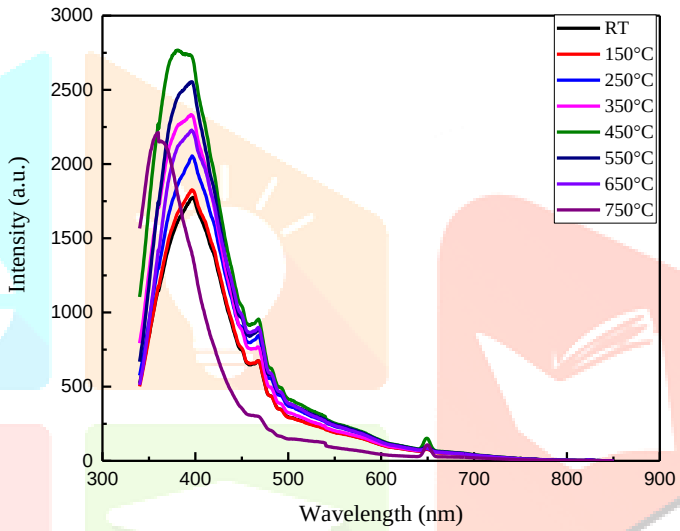

Fig. 10 Intensity- wavelength graph of as-prepared and annealed samples

PL intensity is found to increase with increase in temperature up to 450^0C and then decreases due to the self-trapping mechanism. This is due to the strong coupling between the lattice and the electronic part of excitation in CeO_2. When photons incident on the sample, electrons in the valance band absorbs energy from the photon and get excited to some localized levels and form small polarons. Thus formed polarons and holes interact with each other and result in self-trapping excitation process. From the XRD studies, it is clear that the grain size slightly increases thereby binding energy decreases and it increases the radiative life time. So there is a possibility of self-trapping excitation mechanism.

3.8 Electrical studies

The dielectric constant is evaluated using the equation,

$$\varepsilon_r = \frac{Cd}{\varepsilon 0 A} \qquad (6)$$

Where d is the thickness, A is the area of the sample. Dielectric constant of the as-prepared cerium oxide nanoparticle is 5.738 at a frequency of 0.1011×10^6Hz. Dielectric constant of the as-prepared cerium oxide is high at low frequencies and decreases to higher frequency region at all temperatures. It is due to effect of increased ion jump orientation and the increased space charge polarization properties exhibited by the as-prepared nanoparticles. Figure (11a) shows the frequency dependence of real part of dielectric constant of cerium oxide. At lower frequencies the dielectric constants for all the samples show dispersion, so the dielectric constant is high. From this figure, as the frequency increases dielectric constant decreases, further it becomes constant at higher frequencies (Prabaharan et al. 2016). This is due to the presence of Maxwell Wagner type interfacial polarization. According to this model, heterogeneous microstructure of polycrystalline ceramic consists of semiconducting grains separated by insulating grain boundary. As a result of charge trapping, most of the atoms in the grain boundary become electrically active and generate a dipole moment. At low frequency, dipole moment changes with the applied electric field. So the dielectric constant increases through space charge polarization and rotational polarization. Oxygen vacancies in the sample create space charge at the interface between the sample and electrodes and forms space charge polarization. This electronic polarization leads to high value of dielectric constant at low frequencies. As the frequency increases, space charge polarization due to electric field decreases, it decreases the dielectric constant

(Samuel et al. 2011). From this figure, it is clear that the dielectric constant of the sample increases only up to 310K and then begins to decrease. It is due to the decrease of polarization effect in the applied electric field and thereby dielectric constant decreases.

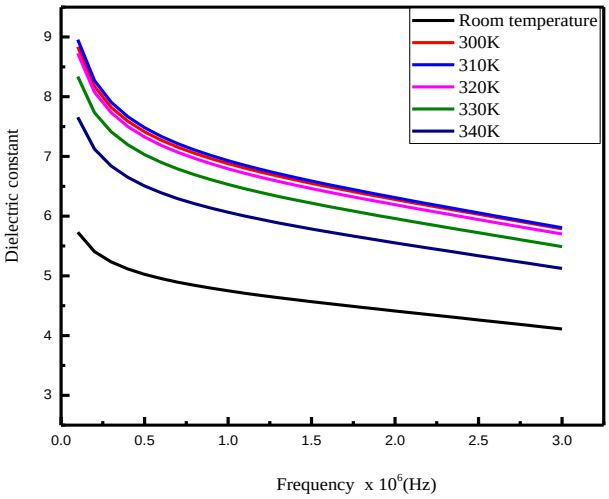

(a) Dielectric constant with frequency

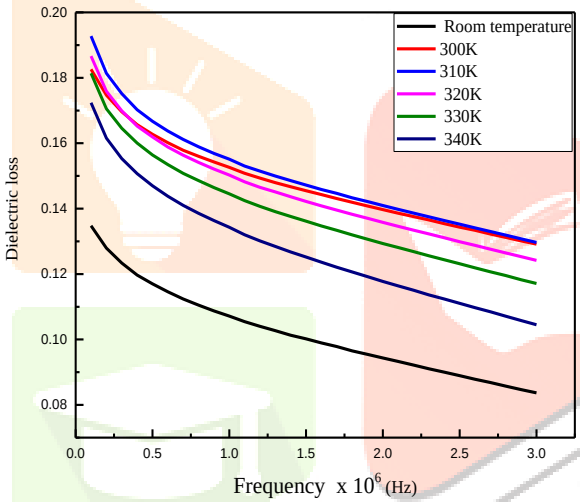

(b) Dielectric loss with frequency

Figure 11: Dielectric constant and Dielectric loss of the as-prepared and annealed samples with frequency

Figure (11b) shows the dependence of dielectric loss with frequency. The as prepared sample shows high dielectric loss at low frequencies and further it decreases to higher frequency region at all temperatures (Sagadevan et al. 2013). Conduction loss, dipole loss, vibrational loss are the three losses associated with dielectric. At the low-frequency region, dielectric loss increases due to the contribution of ion jump, conduction loss of ion migration and ion polarization. The dielectric loss decreases at higher frequency because ion vibration is the only source of dielectric loss at higher frequency. When the temperature increases ac conductivity increases and this leads an increase in dielectric loss. When the temperature increases, dielectric constant & dielectric loss increases up to 310K and then begins to decrease. When the temperature is below Tc, both the values increases due to polarization effect arising from the easy orientation of the dipole. But when the temperature increases above Tc there is a decrease in dielectric constant and dielectric loss due to the thermal oscillation of the molecule and an increase of the degree of disorder of the dipole.

Ac conductivity of the as-prepared sample is shown in figure (12a). AC conductivity of the cerium dioxide Nanoparticle is calculated using,

$$\sigma = 2\pi\epsilon 0\epsilon rf\ tan\theta$$

The transport behavior of the as-prepared sample is studied by characterizing with frequency and temperature dependence of ac conductivity. Ac conductivity of the as-prepared sample is found to be 9.35×10^{-6}S/m for a frequency of 0.1011×10^{6}Hz. From figure (12a), it is clear that the conductivity of the as-prepared sample increases continuously with increase in frequency. It is due to the presence of leakage current. Space charge limited conduction due to the oxygen vacancies and field assisted ionic conduction due to polaron hopping are the two conduction mechanism associated with leakage current. As the frequency increases, space charge polarization due to the electric field decreases and conductivity increases (Suresh et al. 2014). Due to the formation of polaron, movement of the further charge carriers decreases; therefore, electrical conductivity decreases after a particular temperature (310K) (Suresh 2013). Figure (12b) shows the variation of impedance with frequency. When frequency increases impedance decreases by the equation,

$$XL = \frac{1}{C\omega} \qquad (8)$$

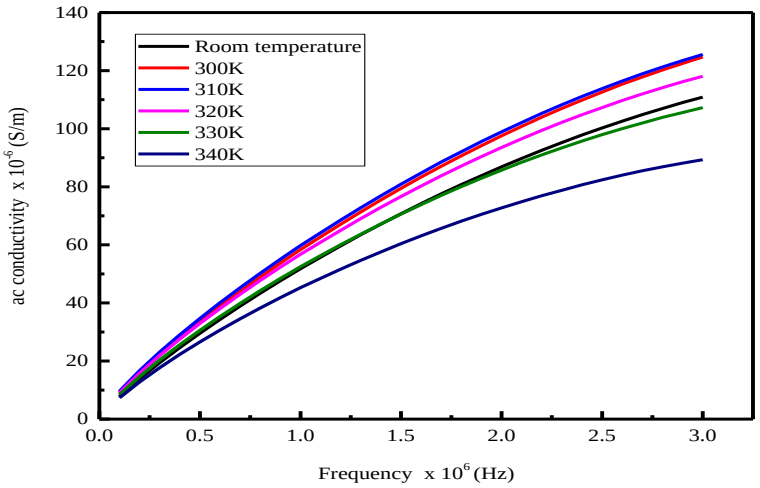

(a) Conductivity with frequency

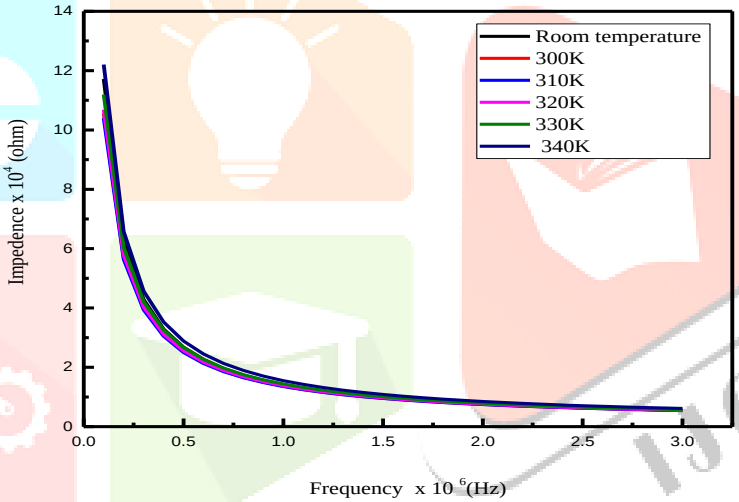

(b) Impedence with frequency

Figure 12: (a) Ac conductivity and (b) Impedence of the as-prepared and annealed samples with frequency

4 Conclusion

Cerium oxide nanoparticles are synthesized using egg white assisted microwave irradiation method. The microwave irradiation with ovalbumin takes less time for the formation of nanoparticles. The as-prepared samples are annealed at different temperatures up to 750^0C. The XRD, TEM and SEM results confirm the presence of rectangular rod-like cerium oxide nanoparticles. Particle size increases and the lattice parameter decreases with increase in temperature. UV-Vis studies confirm well-defined absorption peaks around 320nm. Intensity of Photoluminescence peaks increases with increase in temperature up to 450^0C and then decreases with self- trapping excitation process. The dielectric constant of the as-prepared sample continuously decreases with increase in frequency and gives information about the formation of space charge polarization at low frequencies. The dielectric loss decreases continuously with increase in frequency and it gives the information about the resistance developed at the grain boundaries. AC conductivity increases continuously with the increase in frequencies and as the temperature increases, it increases up to 310K then decreases due to the formation of polarons.

5. Acknowledgment

The authors wish to thank Tequip phase-III seed money Project for providing financial support. Also, thanks to the Department of Physics NIT Trichy for providing the opportunity to undertake the Photoluminescence (PL) study, STICK, Cochin for providing facilities for characterization.

References

1. Yang, Z., Zhou, K., Liu, X., Tian, Q., Lu, D., Yang, S., 2007 Single-crystalline ceria nanocubes: size-controlled synthesis, characterization and redox property. Nanotechnology 18,185606.

2. Chen, H.I., Chang, H.Y., 2004. Homogeneous precipitation of cerium dioxide nanoparticles in alcohol/water mixed solvents. Colloids and Surfaces A: Physicochemical and Engineering Aspects 242, 61–69.

3. Singh, A.V., Bandgar, B.M., Kasture, M., Prasad, B., Sastry, M., 2005. Synthesis of gold, silver and their alloy nanoparticles using bovine serum albumin as foaming and stabilizing agent. Journal of Materials Chemistry 15, 5115–5121.

4. Kargar, H., Ghazavi, H., Darroudi, M., 2015. Size-controlled and bio-directed synthesis of ceria nanopowders and their invitro cytotoxicity effects. Ceramics International 41, 4123–4128.

5. LOGESWARAN, T., PARTHIBAVARMAN, M., 2013. Synthesis of albumen (eggwhite) assisted sno_2 nanoparticles by microwave irradiation method. NanoVision3.

6. Dhannia, T., Jayalekshmi, S., Kumar, M.S., Rao, T.P., Bose, A.C., 2009. Effect of aluminium doping and annealing on structural and optical properties of cerium oxide nanocrystals. Journal of Physics and Chemistry of Solids 70, 1443–1447.

7. Dhannia, T., Jayalekshmi, S., Kumar, M.S., Rao, T.P., Bose, A.C., 2010. Effect of iron doping and annealing on structural and optical properties of cerium oxide nanocrystals. Journal of Physics and Chemistry of Solids 71(7) (2010)

8. Cullity, B.D., 1978. Elements of x-ray diffraction, addison. Wesley Mass.

9. Morris, V., Farrell, R., Sexton, A., Morris, M., 2006. Lattice constant dependence on particle size for ceria prepared from a citrate sol-gel, in: Journal of Physics: Conference Series, p.119.

10. Li, Y.X., Chen, W.F., Zhou, X.Z., Gu, Z.Y., Chen, C.M., 2005. Synthesis of ceo2 nanoparticles by mechanochemical processing and the inhibiting action of nacl on particle agglomeration. Materials Letters 59, 48–52.

11. Yan, M., Wei, W., Zuoren, N., 2007. Influence of ph on morphology and formation mechanism of ceo2 nanocrystalline. Journal of Rare Earths 25, 53–57.

12. Hu, C., Zhang, Z., Liu, H., Gao, P., Wang, Z.L., 2006. Direct synthesis and structure characterization of ultrafine ceo2 nanoparticles. Nanotechnology 17, 5983.

13. Theivasanthi, T., Alagar, M., 2012. Konjac bio-molecules assisted, rod-spherical shaped lead nanopowder synthesized by electrolytic process and its characterization studies. arXiv preprint arXiv: 1212.5795.

14. Sujana, M., Chattopadyay, K., Anand, S., 2008. Characterization and optical properties of nano-ceria synthesized by surfactant-mediated precipitation technique in mixed solvent system. Applied Surface Science 254, 7405–7409.

15. Dos Santos, M., Lima, R., Riccardi, C., Tranquilin, R., Bueno, P.R., Varela, J.A., Longo, E., 2008. Preparation and characterization of ceria nanospheres by microwave-hydrothermal method. Materials Letters 62, 4509–4511.

16. Maensiri, S., Masingboon, C., Laokul, P., Jareonboon, W., Promarak, V., Anderson, P.L., Seraphin, S., 2007. Egg white synthesis and photoluminescence of plate like clusters of ceo2 nanoparticles. Crystal growth & design7, 950–955.

17. Krishnan, A., Sreeremya, T.S., Murray, E., Ghosh, S., 2013. One-pot synthesis of ultra-small cerium oxide nanodots exhibiting multi-colored fluorescence. Journal of colloid and interface science 389, 16–22.

18. Chen, H.I., Chang, H.Y., 2005. Synthesis of nanocrystalline cerium oxide particles by the precipitation method. Ceramics International 31, 795–802.

19. Zhang, D.E., Ni, X.M., Zheng, H.G., Zhang, X.J., Song, J.M., 2006. Fabrication of rod-like ceo2: characterization, optical and electrochemical properties. Solid State Sciences 8, 1290–1293.

20. Phoka, S., Laokul, P., Swatsitang, E., Promarak, V., Seraphin, S., Maensiri, S., 2009. Synthesis, structural and optical properties of ceo2 nanoparticles synthesized by a simple polyvinyl pyrrolidone (pvp) solution route. Materials Chemistry and Physics 115, 423–428

21. Truffault, L., Ta, M.T., Devers, T., Konstantinov, K., Harel, V., Simmonard, C., Andreazza, C., Nevirkovets, I.P., Pineau, A., Veron, O., etal., 2010. Application of nanostructured ca doped ceo2 for ultraviolet filtration. Materials Research Bulletin 45, 527–535.

22. Sathyamurthy, S., Leonard, K.J., Dabestani, R.T., Paranthaman, M.P., 2005. Reverse micellar synthesis of cerium oxide nanoparticles. Nanotechnology 16, 1960.

23. Patsalas, P., Logothetidis, S., Sygellou, L., Kennou, S., 2003. Structure-dependent electronic properties of nanocrystalline cerium oxide films. Physical Review B 68, 035104.

24. Prabaharan, D.M.D.M., Sadaiyandi, K., Mahendran, M., Sagadevan, S., 2016. Structural, optical, morphological and dielectric properties of cerium oxide nanoparticles. Materials Research 19, 478–482.

25. Samuel, M.S., Koshy, J., Chandran, A., George, K., 2011. Electrical charge transport and dielectric response in zno nanotubes. Current Applied Physics 11, 1094–1099.

26. Sagadevan, S., 2013. Synthesis and electrical properties of tio2 nanoparticles using a wet chemical technique. American Journal of Nanoscience and Nanotechnology 1, 27–30.

27. Suresh, S., 2013. Synthesis, structural and dielectric properties of zincsulfide nanoparticles. International Journal of Physical Sciences 8, 1121– 1127.

28. Suresh, S., Arunseshan, C., 2014. Dielectric properties of cadmium selenide (cdse) nanoparticles synthesized by solvothermal method. Applied Nanoscience 4, 179–184.